A METHOD OF LOSS ESTIMATION
FOR
LOW SPEED WIND TUNNELS

by

Frederick B. Bowling

A Thesis Submitted to the Faculty of the

DEPARTMENT OF MECHANICAL ENGINEERING

In Partial Fulfillment of the Requirements
For the Degree of

MASTER OF SCIENCE

In the Graduate College

THE UNIVERSITY OF ARIZONA

1 9 6 3

STATEMENT BY AUTHOR

This thesis has been submitted in partial fulfillment of requirements for an advanced degree at The University of Arizona and is deposited in the University Library to be made available to borrowers under rules of the Library.

Brief quotations from this thesis are allowable without special permission, provided that accurate acknowledgment of source is made. Requests for permission for extended quotation from or reproduction of this manuscript in whole or in part may be granted by the head of the major department or the Dean of the Graduate College when in their judgment the proposed use of the material is in the interests of scholarship. In all other instances, however, permission must be obtained from the author.

SIGNED: Frederick B Bowling

APPROVAL BY THESIS DIRECTOR

This thesis has been approved on the date shown below:

M. R. Bottaccini
Professor of Mechanical Engineering

2 Aug. 63
Date

ACKNOWLEDGMENT

The author gratefully acknowledges the assistance given him by Professor M. R. Bottaccini of the Department of Mechanical Engineering of the University of Arizona. Without his guidance and encouragement this paper would never have been completed.

TABLE OF CONTENTS

ABSTRACT

In this paper a simplified method of estimating the energy losses of low speed, closed circuit wind tunnels of other than circular cross-section is proposed. Only the aerodynamic energy ratio, the ratio of the aerodynamic energy at the test section to the sum of the circuit losses, is considered.

The hydraulic radius is used to define an equivalent diameter, an equivalent angle of expansion, and an equivalent angle of contraction so that use can be made of the existing knowledge of pipe flow theory. Expressions are derived for the loss at each section, then these losses are expressed in coefficient form as a fraction of the aerodynamic energy at the test section. The validity of the method was checked by a series of tests on the one-foot wind tunnel of the Department of Mechanical Engineering, University of Arizona, and some confirmatory results are given.

The experiments indicate that the key to successful loss estimation by the proposed method is the proper evaluation of the nature of surface roughness, particularly in the smaller, higher velocity sections where small errors greatly affect the energy ratio.

CHAPTER 1

INTRODUCTION

1.1 The Problem

The nature of turbulent flow through pipes has been investigated extensively in the past due to its great practical importance. Wattendorf[1] in his study of the Tsing Hua wind tunnel introduced a rational method of applying smooth pipe theory to estimate losses in a closed circuit wind tunnel of circular cross section. The Wattendorf study suggested this paper, the purpose of which will be to propose a technique of extending the Wattendorf method to include wind tunnels of other than circular cross section and the effects of surface roughness.

1.2 Applicability

This problem has practical applications in that no modern wind tunnels are wholly of circular cross section, and particularly in smaller tunnels, 1 to 3 ft. in diameter, the nature of surface roughness has a definite significance. Also, in this age of high construction cost any reasonable approach to more accurate estimates in the preliminary design

phase of low velocity wind tunnels is worthy of thorough investigation.

1.3 Limitations

This study will be confined to general utility, closed circuit type wind tunnels with closed test section since a study of this type wind tunnel introduces most of the basic design problems. Also, flow velocities will be restricted so that compressibility effects can be neglected. As a further limitation the performance of the fan-straightener system and the power supply system will not be considered.

1.4 General Approach

A schematic diagram of a closed circuit, single return wind tunnel is given in Figure 1.1. As proposed by Wattendorf, the tunnel will be broken down for detailed study into four basic components, constant area sections, converging sections, expanding sections, and corners. By using basic techniques a method of computing losses in each section will be proposed. The section losses will be compared to the aerodynamic energy at the test section as a measure of the wind tunnel performance. Finally, the validity of the proposed method will be evaluated on the one foot wind tunnel of the Department of Mechanics, University of Arizona.

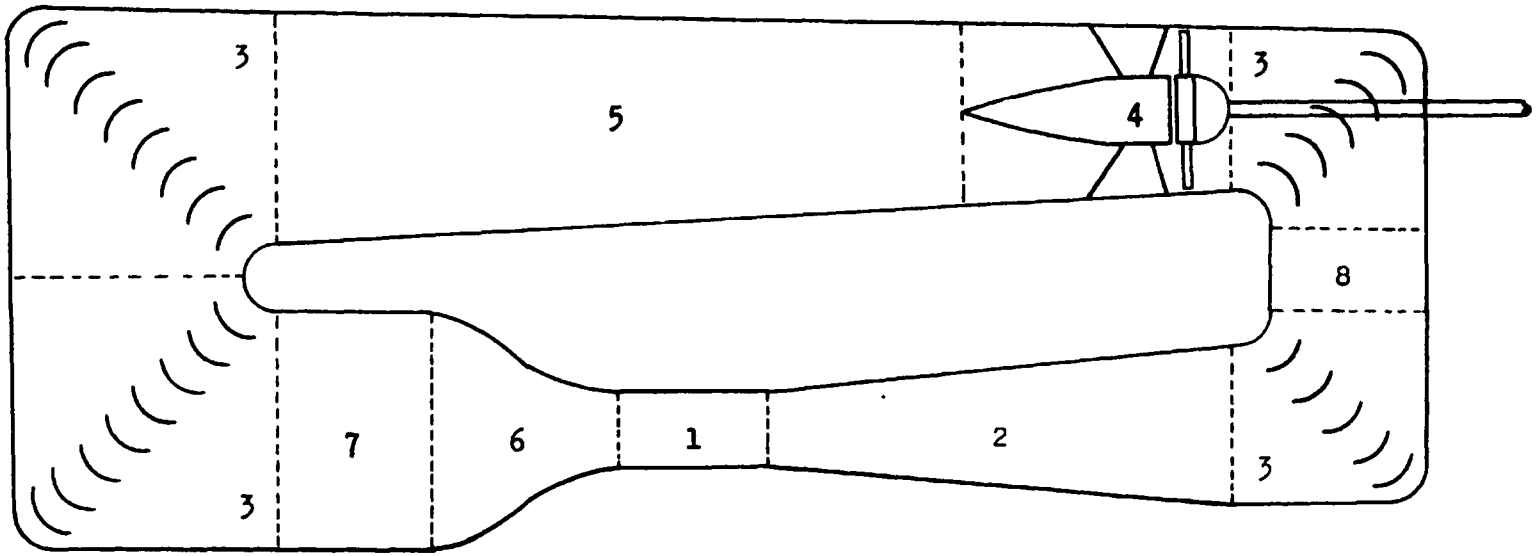

Nomenclature

1. Test Section
2. Diffuser
3. Corner
4. Fan-Straightener System
5. Return Passage
6. Nozzle
7. Settling Chamber

Section Breakdown for Analysis

Constant Area - 1,4,7,8
Expanding - 2,5
Contracting - 6
Corners - 3

Figure 1.1 Schematic Diagram of a Low Speed Wind Tunnel

CHAPTER 2

FLUID FRICTION

2.1 The Nature of Friction Losses

The nature of friction losses in ducted flow can be best described by considering fully developed steady flow in a straight duct of constant circular cross-section. The cylinder of fluid shown in Figure 2.1 is not subject to any inertia forces, so the condition of equilibrium can be expressed as a balance between static pressure forces and forces due to shear stress on the circumference in the form

$$\tau = \frac{p_1 - p_2}{L} \frac{r}{2} \qquad (2.1)$$

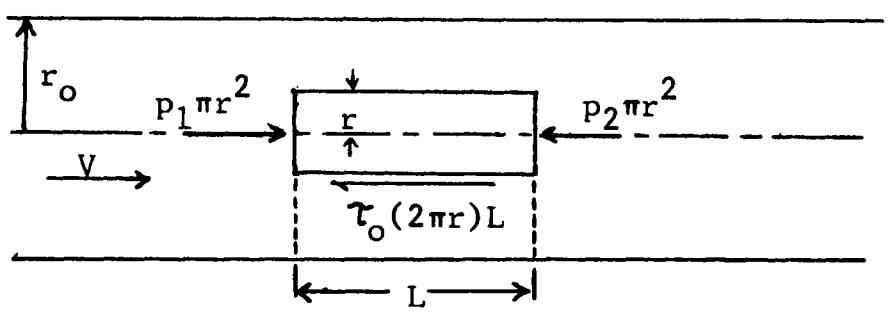

Figure 2.1 Steady flow through circular duct

where τ is the sum of the laminar and turbulent shear stress.

This indicates that the presence of fluid friction causes a drop in static pressure.

2.2 Coefficient of Friction

Equation 2.1 is equally valid for laminar and turbulent flow since τ is taken to be the apparent shear stress, that is the sum of laminar and turbulent shearing stress. For the case of the pure laminar flow through a circular duct the relationship between the shear stress, pressure gradient, and average velocity* can be determined theoretically by use of Newton's law of viscosity,

$$\tau = - \mu \frac{du}{dr} \qquad (2.2)$$

For turbulent flow the relationship must be obtained empirically since attempts to solve theoretically even a particular case of turbulent flow have failed. There is a wealth of literature that contains a number of empirical "laws of fluid friction." Some of these equations introduce coefficients that depend on a particular system of units and are unwieldy for general use; examples of these are the Manning n and Chezy C^2.

---

*Average velocity is defined as $V = \frac{1}{A}\int_A u \, d\, A$ where A is the cross-section area of the duct and u is the fluid velocity at the elemental area d A.

It is now common to express the pressure gradient for incompressible flow in the form of the so-called Darcy-Weisbach equation.

$$\frac{P_2 - P_1}{L} = \frac{f}{D} \frac{\rho V^2}{2} \tag{2.3}$$

Where f is a dimensionless "friction" coefficient, $\rho V^2/2$ is dynamic pressure of the mean flow and D is the diameter of the pipe. A comparison of Eq. 2.2 and Eq. 2.4 give the relationship between the wall shear stress and the friction factor.

$$\tau_o = f \frac{\rho V^2}{8} \tag{2.4}$$

The friction factor is often defined as the ratio of the local wall shear stress to the dynamic pressure of the mean flow.

$$C_f = \frac{\tau_o}{\rho V^2/2} \tag{2.5}$$

from which it follows that the Darcy-Weisbach coefficient is four times this value. To avoid confusion only the Darcy-Weisbach f will be used for the rest of this paper.

From the wealth of research[3] that has been done in evaluating the coefficient it has been determined that it varies in a complex manner as a function of the velocity of flow, the fluid density and viscosity, the pipe diameter

and the nature of the surface roughness. One of the most thorough compilations of the empirical results of the research is the Moody diagram which is a log-log plot of f as a function of Reynolds number, VD/ν, and relative roughness, e/D; where V is the mean flow velocity, and D is the pipe diameter, ν is the fluid kinematic viscosity and e, the absolute roughness, is the equivalent size of the surface roughness projections based on Nikuradse's sand grain experiments. The Moody diagram is convenient to use in pipe loss computations because it covers laminar flow and fully developed turbulent flow for hydraulically smooth boundaries, completely rough boundaries, and the transition area between the two.

2.3 Coefficient of Friction for Ducts not of Circular Cross-Section

In the study of open channel flow extensive use is made of the hydraulic radius, m, which is defined as the ratio of the cross-section area, A, of the fluid flowing in the channel to the wetted perimeter, P, of the channel,

$$m = A/P \tag{2.6}$$

Skoglund[4] conducted a series of experiments to determine the behavior of the coefficient of friction in the flow of air through artifically roughened, closed ducts of rectangular

cross-section. As a result of his experiments, Skoglund concluded that the coefficient of friction for turbulent flow in rectangular ducts can be estimated by using the pipe flow law with 4m, instead of the pipe diameter, as the characteristic dimension of the duct with an error of less than one-half per cent. This leads to the assumption that by transforming a duct, not of circular cross-section, into an equivalent cylindrical duct of diameter, D_e, such that,

$$D_e = 4m = 4 \frac{A}{P} \qquad (2.7)$$

the coefficient of friction can be read directly from the Moody diagram if the nature of the surface roughness of the duct is known.

CHAPTER 3

EXPRESSIONS FOR DUCT LOSSES

3.1 Friction Losses in Ducts of Constant Cross-Section

For the case of steady flow in a constant area duct an expression for the friction losses can be developed by using the momentum-flux force principle and the definitions of Chapter 2.

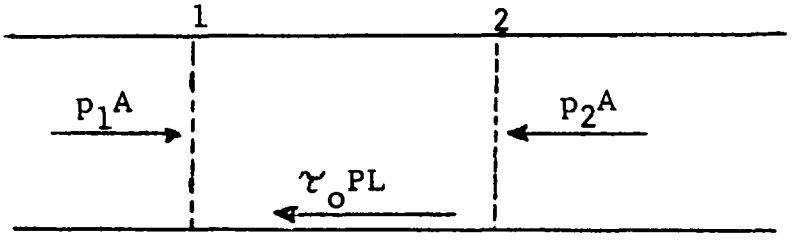

Figure 3.1 Forces on a section of fluid in steady flow.

From Figure 3.1

$$(P_1 - P_2)A = \tau_o PL \qquad (3.1)$$

where A is the cross-section area and P and L are the perimeter and length respectively. On introducing the relationship between the friction factor and the shear stress from Eq. 2.5 and the definition of the equivalent

diameter from Eq. 2.8, Eq. 3.1 becomes

$$\Delta P = f \frac{L}{D_e} \frac{\rho V^2}{2} \tag{3.2}$$

which, as might be expected, is similar to the Darcy-Weisbach equation.

3.2 Losses at an Expansion

It is reasonable to expect that there will be a decrease in losses at an expansion due to the decrease in velocity; however, this is not the case.[5] The nature of the reaction at the duct walls is such that an effective pressure force is added to the frictional force. If the expansion occurs too rapidly, the adverse pressure gradient will cause the flow to separate from the walls resulting in excessive losses. Because of the different nature of the two types of losses it is advantageous to consider them separately as friction losses Δp_f and expansion losses Δp_x.

a. Friction losses

The basic ideas of Chapter 2 are not so readily applied at an expansion for ducts not of circular cross-section as they are in the case of constant area ducts. It is convenient then to consider first a cylindrical expansion. Eq. 3.1 can be written

$$\Delta p_f = \int_L \frac{f}{4} \frac{\rho V^2}{2} \frac{P}{A} \, ds \tag{3.3}$$

where s is measured along the surface of the duct. (See Figure 3.2).

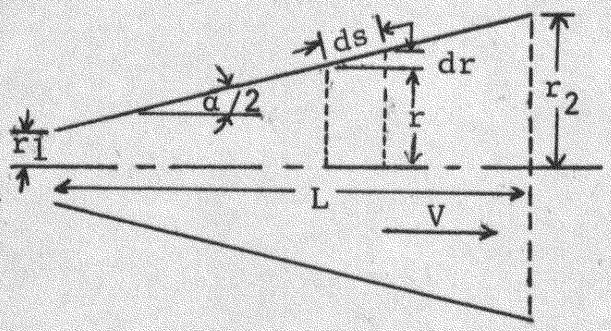

Figure 3.2 Duct expansion

From the continuity equation $V = V_1A_1/A$, $A = \pi r^2$, $p = 2\pi r$, $ds = dr/\tan \alpha/2$ for $\alpha < 10°$, and assuming an average value for f, Eq. 3.3 becomes

$$\Delta p_f = \frac{f}{8\tan(\alpha/2)} \cdot \frac{\rho}{2} (V_1^2 - V_2^2) \qquad (3.4)$$

A logical extension of this to include other cross-sections is to write Eq. 3.3 in terms of equivalent diameters and proceed as above. If this is done, the continuity of velocity will be lost because areas based on equivalent diameters are equal to actual areas only for circular cross-sections. Since friction losses vary as velocity squared, it will be wise to use the actual velocities in loss computations.

On comparing Eq. 3.2 and the Darcy-Wesibach equation it will be noted that the only difference between the two is

the length term in the denominator. The Darcy-Weisbach form uses the actual inside pipe diameter, but Eq. 3.2 uses the equivalent diameter. This observation leads to the assumption of an equivalent angle of expansion defined as

$$\beta/2 = \tan^{-1} \frac{1/2(De_2 - De_1)}{L} \qquad (3.5)$$

This assumption seems reasonable in that the accuracy of using De to select f has been established by Skoglund and the angle β provides the relationship between De_1 and De_2 that the angle α gives for D_1 and D_2 in pipe flow. Applying the equivalent angle of expansion to Eq. 3.4 gives, as an expression for the friction losses in a duct of other than circular cross-section,

$$\Delta p_f = \frac{f}{8 \tan (\beta/2)} \rho/2(V_1^2 - V_2^2) \qquad (3.6)$$

where V_1 and V_2 are the average velocities based on the actual areas at section 1 and section 2.

b. Expansion Losses

Wattendorf,[1] by assuming linear velocity profiles in the retarded layer of fluid near the duct walls, arrived at the following expression for the expansion losses in a cylindrical expansion:

$$\Delta p_x = \frac{4}{3} \tan \frac{\alpha}{2} \frac{\rho}{2}(V_1^2 - V_2^2) \qquad (3.7)$$

Wattendorf checked this expression in a series of tests in the Tsing Hua 10-foot wind tunnel and found that the losses were over-estimated. As a result of his experiments he arrived at

$$\Delta p_x = 0.6 \tan \frac{\alpha}{2} \frac{\rho}{2}(V_1^2 - V_2^2) \qquad (3.8)$$

for α less than 10 degrees. By reasoning similar to that used in the development of friction losses, it will be assumed Eq. 3.8 can be extended to include ducts of other than circular cross-section by using the equivalent angle of expansion defined by Eq. 3.5. Thus the expansion loss expression becomes

$$\Delta p_x = 0.6 \tan \frac{\beta}{2} \frac{\rho}{2}(V_1^2 - V_2^2) \qquad (3.9)$$

The total loss at an expansion is simply the sum of the friction and expansion losses, that is,

$$\Delta p = \left[\frac{f}{8 \tan (\beta/2)} + 0.6 \tan \frac{\beta}{2}\right] \frac{\rho}{2}(V_1^2 - V_2^2) \qquad (3.10)$$

3.3 Losses at a Contraction

In the design of wind tunnel nozzles[6,7] a major consideration is to avoid adverse pressure gradients in the

contraction cone. Therefore, it is reasonable to assume that the losses at a nozzle are due to friction alone, so that Eq. 3.3 is applicable.

$$\Delta p = \int_L \frac{f}{4} \frac{\rho}{2} V^2 \frac{p}{A} \, ds \qquad (3.11)$$

Due to the complex surface contours inherent in nozzle shapes Eq. 3.11 is not amenable to general solution, but should be solved for individual nozzle. Wattendorf by assuming as average value for the coefficient of friction solved Eq. 3.11 for cylindrical nozzles of contraction ratios varying from 4 to 11 and gives as an average solution

$$\Delta p = 0.32 \, f \, \frac{L}{D} \frac{\rho}{2} V^2 \qquad (3.12)$$

where L is the length of the contraction cone and D and V are the diameter and velocity at the exit of the nozzle. Pope, observing that nozzle losses seldom reach 3 per cent of total wind tunnel losses, reasons that small errors in approximating nozzle losses will have a negligible effect in the estimation of over-all tunnel performance.

There is ample evidence to accept the validity of Eq. 3.12 as, at worst, a good first approximation of the losses at a nozzle in a cylindrical wind tunnel; and to extend the application to other than circular cross-sections by introducing the equivalent diameter of Eq. 2.9, so that Eq. 3.12 becomes

$$\Delta p = 0.32f \frac{L}{De} \frac{\rho}{2} V^2 \qquad (3.13)$$

where f is the average coefficient of friction between the contraction entrance and exit and De and V are respectively the equivalent diameter and actual average velocity at the exit.

Normally a contraction of the wind tunnel circuit other than at the nozzle is to be avoided because losses increase as the square of the velocity. However, it is not inconceivable that such a contraction might be necessary. If such a contraction is encountered, by assuming that the losses are due only to friction effects, Eq. 3.11 can be integrated by using an average value of the coefficient of friction to yield an expression similar to that for friction losses at an expansion. The drop in pressure at a contraction is

$$\Delta p = \frac{f}{8 \tan \theta/2} \frac{\rho}{2}(V_2^2 - V_1^2) \qquad (3.14)$$

where θ is the equivalent angle of contraction defined by

$$\frac{\theta}{2} = \tan^{-1} \frac{1/2(De_1 - De_2)}{L} \qquad (3.15)$$

3.4 Losses at Corners

In a closed circuit wind tunnel the air stream must be turned 360 degrees. Although this can be done

different ways, the most generally accepted manner is to employ two sets of two similar 90 degree turns. Since each turn can generate a loss of as much as a complete velocity head, a cascade of turning vanes is normally included at each corner to minimize the loss.

To determine the profile of an individual turning vane consider the steady flow of a non-viscous fluid. For an infinite row of vortices of equal strength, γ, spaced an equal distance, a, apart along the x axis with the center vortex at the origin as shown in Figure 3.3a, the stream function is

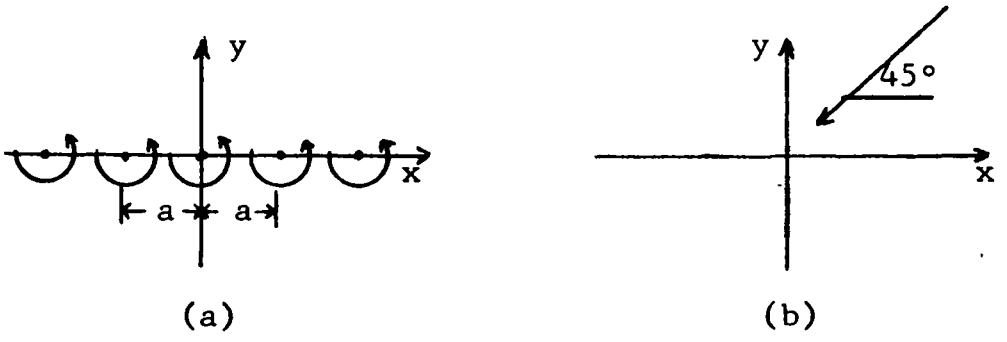

Figure 3.3 Components of flow around corners.

$$\psi_1 = \frac{\gamma}{2} \ln 1/2(\cosh \frac{2\pi y}{a} - \cos \frac{2\pi x}{a}) \qquad (3.16)$$

For a uniform velocity, V, oriented at 45 degrees to the x axis as shown in Figure 3.3b, the stream function, ψ_2, is

$$\Psi_2 = 1\ \frac{\sqrt{2}\ V}{2}\ (x + y) \tag{3.17}$$

By superposition the stream function, Ψ , of the combination of these two flows is

$$\Psi = \Psi_1 + \Psi_2 = \frac{\kappa}{2} \ln 1/2(\cosh \frac{2\pi y}{a} - \cos \frac{2\pi x}{a}) - \frac{\sqrt{2}\ V}{2}(x + y) \tag{3.18}$$

Following the approach of Krober[8] the strength of vortices so that the approach velocity will be turned 90 degrees can be determined. In Figure 3.4 for the approach

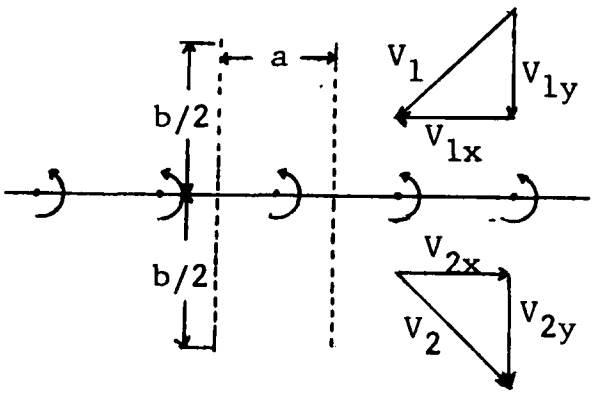

Figure 3.4 Uniform Velocity turned 90 degrees by a vortex row.

velocity to be turned as required

$$V_{1y} = V_{2y} \tag{3.19a}$$

$$V_{1x} = -V_{2x} \tag{3.19b}$$

The required strength is

$$\kappa = \oint (V_{1x}\, dx + V_{1y}\, dy) \tag{3.20}$$

In this case $V_{1y} = V_{2y}$ = a constant and does not contribute to the circulation. Equation 3.20 becomes

$$\kappa = \int_0^{b/2} V_{1x}\, dx + \int_{-b/2}^{0} V_{2x}\, dx = 2\int_0^{b/2} V_{1x}\, dx \tag{3.21}$$

as b tends to infinity.

$$\kappa = 2V_{1x}a = aV_1\sqrt{2} \tag{3.22}$$

Substituting for κ in Equation 3.18 the stream function becomes

$$= \frac{V\sqrt{2}}{2}\left[a \ln 1/2\left(\cosh \frac{2\pi y}{a} - \cos \frac{2\pi x}{a}\right) - (x + y)\right] \tag{3.23}$$

The stream lines appear as a nest of ellipses which indicates that an appropriate turning vane profile should be of elliptical shape.

The required profile for turning vanes has been the subject of much research and experimentation which has resulted in the comprehensive evaluation of several profiles, both thick and thin. Winters[9] found that thin turning vanes function as efficiently as the thick vanes and recommends

their use unless the thick vanes are needed to provide cooling. One of the remarkable results of his work is that a thin vane with the profile of a quadrant of a circle with short tangential extensions, as an approximation of the elliptical shape, reduces corner losses as efficiently as the more complicated aerofoil profiles. The thin circular profile is particularly useful in smaller wind tunnels where economy of fabrication and ease of installation are of considerable importance.

The usual performance indicator for vaned corners is a coefficient expressing the pressure loss across the corner as a fraction of the dynamic pressure at the corner entrance,

$$\Delta p = k \frac{\rho}{2} V^2 \qquad (3.24)$$

For properly designed corners reasonable values[9] of k vary from 0.15 to 0.21 at Reynolds numbers, referred to the vane chord, of 10^4 to 10^5.

It has been determined that only about one-third of the corner losses is due to surface friction so that the remaining two-thirds is probably caused by secondary flows induced by the vanes in rotating the air stream.[5] It is convenient here to consider the two types of losses separately by defining

$$k = k_f + k_r = k/3 + k_r \tag{3.25}$$

where k_f and k_r refer to friction losses and rotation losses respectively.

Considering first the friction losses, it will be assumed that the surface drag on the vanes follows a law[10] similar to that of a smooth flat plate in turbulent flow, so that

$$k_f = b\lambda = b \frac{0.455}{(\log_{10} N_{Re})^{2.58}} \tag{3.26}$$

where N_{Re} is the Reynolds number based on the vane chord and b is a constant to be determined. It is reasonable to assume that the corner design will be based on a previously evaluated profile so that the value of k and the test Reynolds number will be known. Knowing these parameters k_f can be set equal to k/3 and by substitution into Eq. 3.16 the factor b can be determined.

It is customary to assume that the rotational losses are independent of Reynolds number, so that

$$k_r = \frac{2}{3} k \tag{3.27}$$

For use later the corner loss coefficient will be developed here for a corner with turning vane profiles of the quadrant of a circle with short tangential extensions

at each end. For profiles of this type at a test Reynolds number of 2×10^5 a reasonable value of k is 0.15.[9] From Eq. 3.16,

$$b = 0.05 \frac{\log_{10}(2 \times 10^5)^{2.58}}{0.455} = 8.13 \qquad (3.28)$$

and

$$k_f = \frac{3.8}{(\log_{10} N_{Re})^{2.58}} \qquad (3.29)$$

From Eq. 3.27

$$k_r = 2/3(0.15) = 0.10 \qquad (3.30)$$

From which it follows

$$\Delta p = \left[0.10 + \frac{3.8}{(\log_{10} N_{Re})^{2.58}}\right] \frac{\rho}{2} V^2 \qquad (3.31)$$

3.5 Losses at Miscellaneous Fixtures

Wind tunnels often have flow improvement fixtures such as honeycombs and turbulence damping screens. The analysis of flow around these fixtures is beyond the scope of this paper, but experimentally determined performance curves can be found in the literature. As in the case of the turning vanes it is customary to express the loss across these fixtures as a fraction of the approach dynamic pressure. Pope gives curves of pressure drop coefficients

versus approach velocity for 18, 20, 24, and 60 mesh damping screens and average coefficients for rectangular, hexagonal, and circular honeycombs. The equation for the pressure loss at one of these fixtures is

$$\Delta p = k \frac{\rho V^2}{2} \tag{3.32}$$

CHAPTER 4

WIND TUNNEL PERFORMANCE

4.1 Section Energy Losses

As established in Chapter 3 the losses in the various wind tunnel sections occur as a static pressure drop in the section. This drop in pressure appears across the area at the downstream end of the section, and the product of the area and the pressure drop gives the drag force experienced by the section. The product of the drag force and the velocity at the downstream end of the section gives the energy loss across the section which is normally expressed in coefficient form as a function of the dynamic energy at the downstream end of the section. Thus,

$$k = \frac{\Delta pAV}{\frac{\rho}{2}AV^3} = \frac{\Delta p}{\frac{\rho}{2}V^2} \qquad (4.1)$$

where k is the coefficient of energy loss, Δp is the pressure drop across the section, and V is the average velocity at the downstream end of the section.

4.2 Energy Ratio

As a measure of wind tunnel performance, the aerodynamic energy ratio will be used, that is, the ratio of the aerodynamic

energy at the test section to the total energy loss around the wind tunnel circuit,

$$ER = \frac{\frac{\rho}{2} V_t^3 A_t}{\Sigma \text{ Section Losses}} \tag{4.2}$$

The energy loss at each section can be related to the aerodynamic energy at the test section in terms of the section energy loss coefficient by rewriting Eq. 4.1,

$$\text{Section Energy Loss} = k \frac{\rho}{2} AV^3 \tag{4.3}$$

and by introducing the law of continuity to get the local velocity in terms of the test section velocity.

$$\text{Section Energy Loss} = k \frac{\rho}{2} A\left(\frac{A_t V_t}{A}\right)^3 = k \frac{A_t^2}{A^2} \frac{\rho}{2} A_t V_t^3 \tag{4.4}$$

By defining the basic loss coefficient,

$$K_t = k \frac{A_t^2}{A^2} \tag{4.5}$$

Eq. 4.4 becomes

$$\text{Section Energy Loss} = K_t \frac{\rho}{2} A_t V_t^3 \tag{4.6}$$

By substituting Eq. 4.6 into Eq. 4.2, the energy ratio becomes

$$ER = \frac{\frac{\rho}{2} V_t^3 A_t}{\Sigma K_t \frac{\rho}{2} V_t^3 A_t} = \frac{1}{\Sigma K_t} \tag{4.7}$$

Thus the energy ratio can be estimated by tabulating the basic loss coefficient for each of the component sections of the wind tunnel.

It should be emphasized here that this definition of the energy ratio does not include the fan-straightener efficiency nor the power supply efficiency. However, an analysis based on this definition of the energy ratio is necessary in order to estimate the steady flow output to be used in the design of the two omitted components.

4.3 Basic Energy Coefficients

An expression for the basic loss coefficient for a section of constant cross-section area can be derived by using Eqs. 3.2, 4.1, and 4.5. By direct substitution of Eq. 3.2 into Eq. 4.1,

$$k = f \frac{L}{D_e} \tag{4.8}$$

and by substituting Eq. 4.8 into Eq. 4.5 the basic energy loss coefficient becomes

$$K_t = f \frac{L}{D_e} \frac{A_t^2}{A^2} \tag{4.9}$$

By continuing in a similar manner expressions for the basic energy loss coefficient can be obtained. In Table 4.1 is a list of these expressions together with the limitations of their use as developed in Chapter 3.

Section	Basic Energy Loss Coefficient	Remarks
Constant Area	$f \frac{L}{D_e} \frac{A_t^2}{A^2}$	
Expansions	$(\frac{f}{8 \tan \frac{\beta}{2}} + 0.6 \tan \frac{\beta}{2})[\frac{A_2^2}{A_1^2} - 1] \frac{A_t^2}{A_2^2}$	Average f $\beta < 10°$
Contractions	$(\frac{f}{8 \tan \frac{\theta}{2}})[1 - \frac{A_2^2}{A_1^2}] \frac{A_t^2}{A_2^2}$	Average f $\theta < 10°$
Nozzles	$0.32 f \frac{L}{D_e}$	Average f For contraction ratios from 4 to 11
Corners	$[0.10 + \frac{3.8}{(\log_{10} N_{Re})^{2.58}}] \frac{A_t^2}{A^2}$	For thin vanes with profiles of circular quadrant with short tangential extensions N_{Re} referred to vane chord
Miscellaneous Fixtures	$k \frac{A_t^2}{A^2}$	k determined from the appropriate references

Table 4.1 Expressions for the Basic Energy Loss Coefficient, K_t

CHAPTER 5

APPLICATION AND VALIDATION

5.1 Wind Tunnel Description

This method of loss estimation will be used to calculate the static pressure distribution around the one-foot tunnel of the Department of Mechanical Engineering, University of Arizona. This wind tunnel is a vertical, single return, closed circuit tunnel. It is driven by a 7-1/2 horsepower electric motor that operates at a constant rpm of 1750. The motor is connected to the fan through a Cleveland Speed Variator that allows the fan speed to be varied continuously from 580 to 5250 rpm. It has a plastic test section and a metal nozzle with the remainder of the tunnel constructed of one-half inch plywood. The cross-section of the tunnel varies from rectangular at the test section to octagonal at the end of the diffuser, then from octagonal back to rectangular between the first and second corners. The nature of the transition in cross-sectional area between the first and the second corners is such that the flow expands then contracts. This collection of different type flow channels

in one closed circuit provides an excellent test vehicle. A detailed drawing of the tunnel and the appropriate cross-section areas is included in Appendix II.

5.2 Method of Application

To provide a convenient parameter for comparison with test data the dimensionless ratio $(p - p_t)/(1/2\ \rho V_t^2)$ will be computed at the end of each section around the wind tunnel circuit. With compressibility neglected the steady flow energy equation can be written

$$p_t + \frac{\rho V_t^2}{2} + E_A = p + \frac{\rho V^2}{2} + E_L \qquad (5.1)$$

where p_t is the static pressure and V_t is the average velocity at the test section, p is the static pressure and V is the average velocity at any other section, and E_A is the energy added and E_L is the energy lost between the two sections. By introducing the continuity equation and the basic energy coefficient of Chapter 4, Equation 5.1 becomes

$$\frac{p_i - p_t}{\frac{\rho V_t^2}{2}} = 1 - \left(\frac{A}{A_t}\right)^2 - \sum_t^i K_t + E_A \qquad (5.2)$$

Once steady flow has been established, the energy supplied exactly balances the energy losses around the circuit and

in the wind tunnel energy is added only at the fan. By adding the K_t for the complete circuit any time the fan is between the test section and the next section being considered Equation 5.2 can be used to estimate the pressure distribution around the wind tunnel circuit.

The pressure distribution was computed for average test section velocities of 40, 60, 80, and 100 feet per second with an assumed temperature of 80 degrees Farenheit and an average barometric pressure of 27.5 inches of mercury. Friction factors were read from the Moody diagram by assuming the test section to be smooth, the nozzle to have the same absolute roughness as commercial steel, and the remainder of the tunnel to have an average absolute roughness of wood stave as determined by Moody. The results of these computations are tabulated in Appendix III.

5.3 Instrumentation

The instrumentation required to measure the pressure distribution around the tunnel consisted of a pitot-static tube connected across a differential manometer to measure the dynamic pressure at the test section and a bank of manometers to measure the static pressure at key positions around the tunnel. The differential manometer was manufactured by the Ellison Draft Gage Company and could be read directly

in inches of water with an accuracy of $\pm$ 0.01 inches of water. The bank of manometers contained oil with a specific gravity of 0.834 and was inclined at an angle of 31 degrees to the horizontal. Here the scale was in inches and had to be converted to inches of water by multiplying scale readings by the specific gravity of the manometer oil and the sine of the angle of inclination. The manometer bank could be read with an accuracy of $\pm$ 0.01 inches of water.

Piezometric pressure taps were positioned at nine locations as shown in Figure II-1. At each location the taps were connected to make a piezo-ring. Each piezo-ring was connected to a manometer in the bank. The static pressure connection of the pitot-static tube was also connected to one manometer in the bank. By taking the static pressure measured at the pitot-static tube as p_t, the pressure difference in inches of water between a particular piezo-ring and the test section was conveniently obtained by the difference of two manometer readings multiplied by the conversion factor discussed above.

The required dynamic pressure, q, was computed from the relation

$$q = \frac{\rho V^2}{2} \tag{5.3}$$

By expressing the density in terms of pressure and temperature

and introducing the conversion factors to obtain q in inches of water when pressure is in inches of mercury and temperature is in degrees Rankine, Equation 5.3 becomes

$$q = 3.96 \times 10^{-3} \frac{pV^2}{T} \qquad (5.4)$$

This allowed the dynamic pressure to be computed by selecting an average velocity for the test section and reading the local atmospheric pressure and temperature from the mercury barometer and the thermometer located in the laboratory.

5.4 Conduct of the Tests

To determine the nature of the flow at the test section a series of pitot-static traverses were made using a micro-manometer with an accuracy of $\pm$ 0.001 inches of water. This revealed that q continued to increase from the end of the nozzle to the middle of the test section. At this point the ratio of the average q at the cross-section to q measured at the center of the cross-section was 0.995. This point was selected as the location of the pitot-static tube for the remainder of the tests since the flow was fully developed and in light of the accuracy of the instrumentation the ratio of q average to q centerline could be taken as unity. This allowed the test q to be computed directly by Equation 5.4.

Test runs were made for the average test section velocities of 40, 60, 80, and 100 feet per second. The test data and its extension are tabulated in Appendix IV.

5.5 Comparison

In Figures 5.1 - 5.4 are plotted the computed and measured values of the ratio $(p - p_t)/1/2\ pV_t^2$ around the tunnel circuit. Inspection of these curves indicate an acceptable agreement between the calculated and measured pressure distribution. However, Figure 5.5 shows the calculated energy ratio to vary from approximately 20 to 30 per cent higher than the measured energy ratio.

The only two points that showed a consistent deviation occurred at the end of the test section and the end of the diffuser. The major casues of this deviation at the end of the diffuser was the presence of the fan and boss in the flow channel. The boss was located immediately downstream of the pressure tap and effectively presented a flat circular disk normal to the flow that blocked approximately 10% of the flow area. The decrease in area caused the measured static pressure to be lower than the computed value since the presence of the fan-straightener system was neglected in the computations. The major cause of low estimated loss across the test section was the assumption of smooth flow

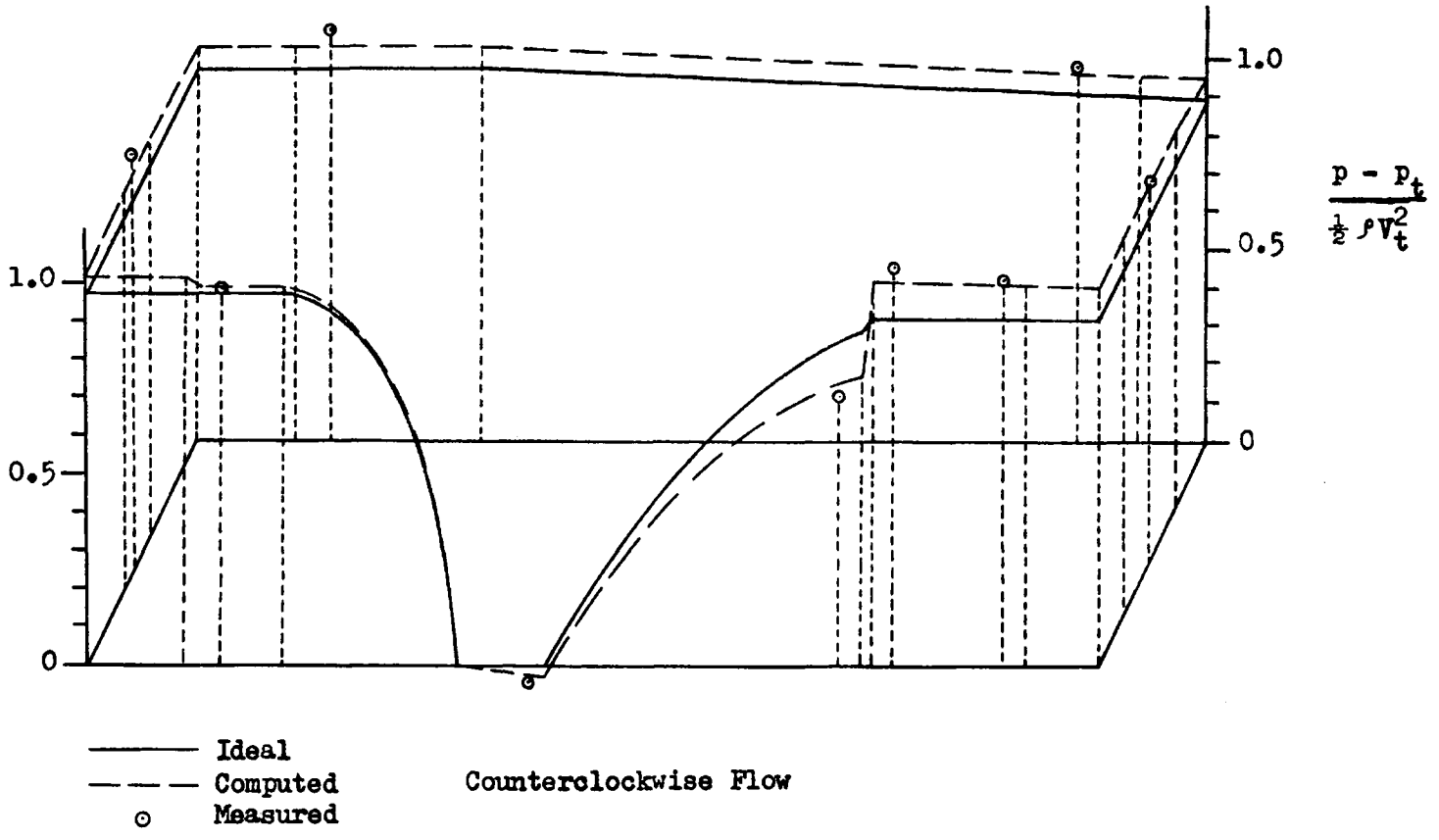

Figure 5.1 Pressure Distribution for Test Section Velocity of 40 fps

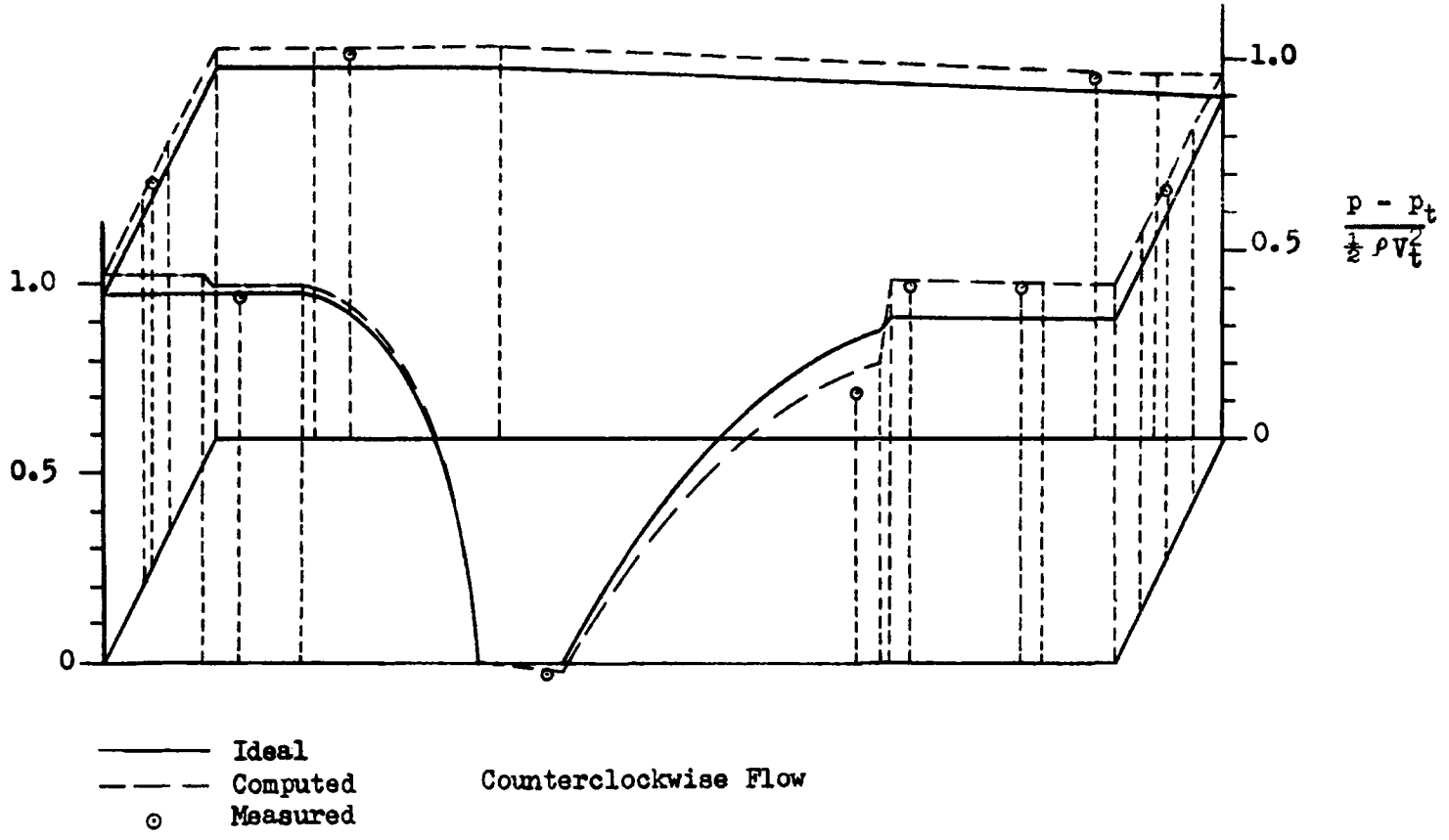

Figure 5.2 Pressure Distribution for Test Section Velocity of 60 fps

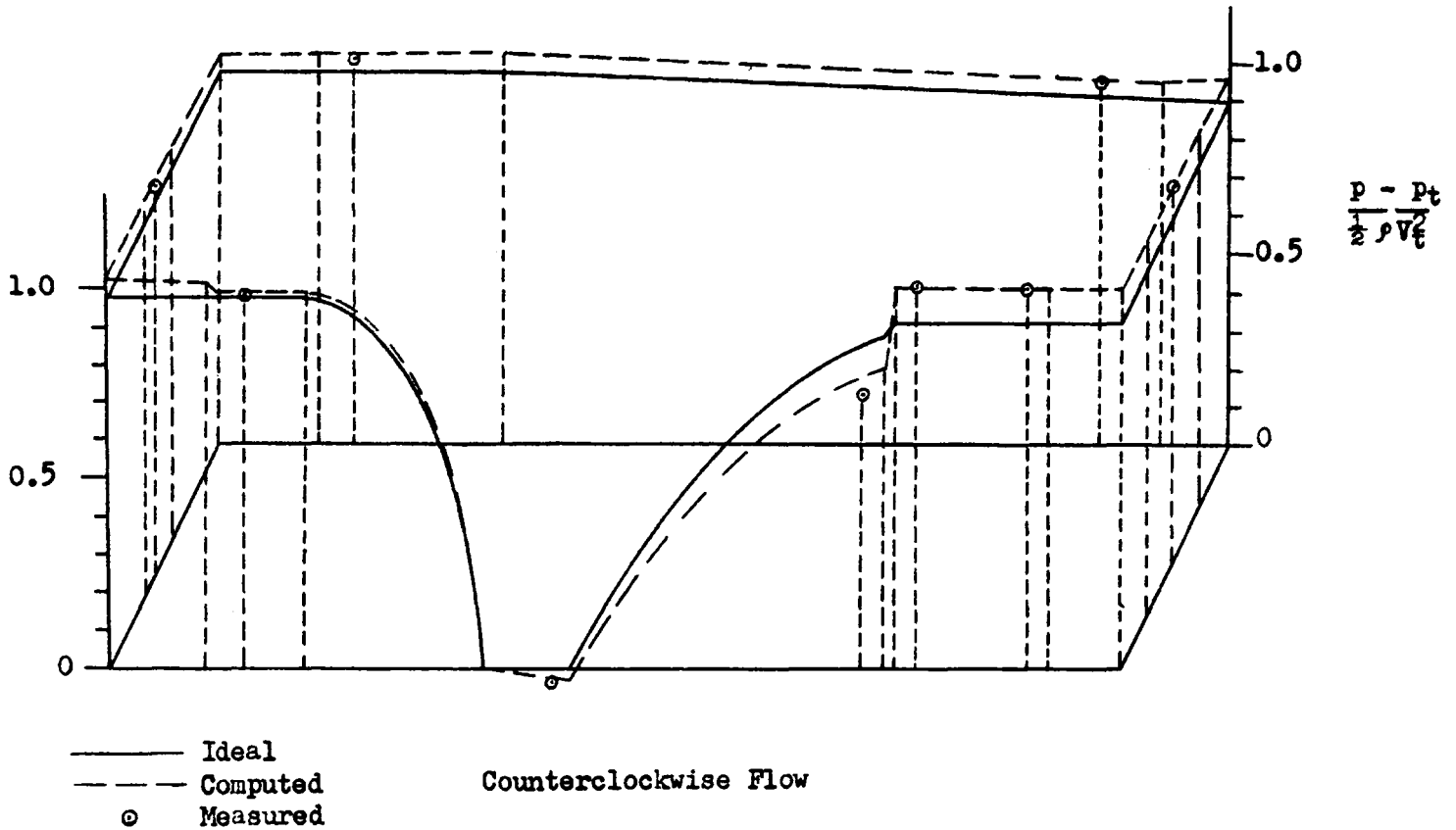

Figure 5.3 Pressure Distribution for Test Section Velocity of 80 fps

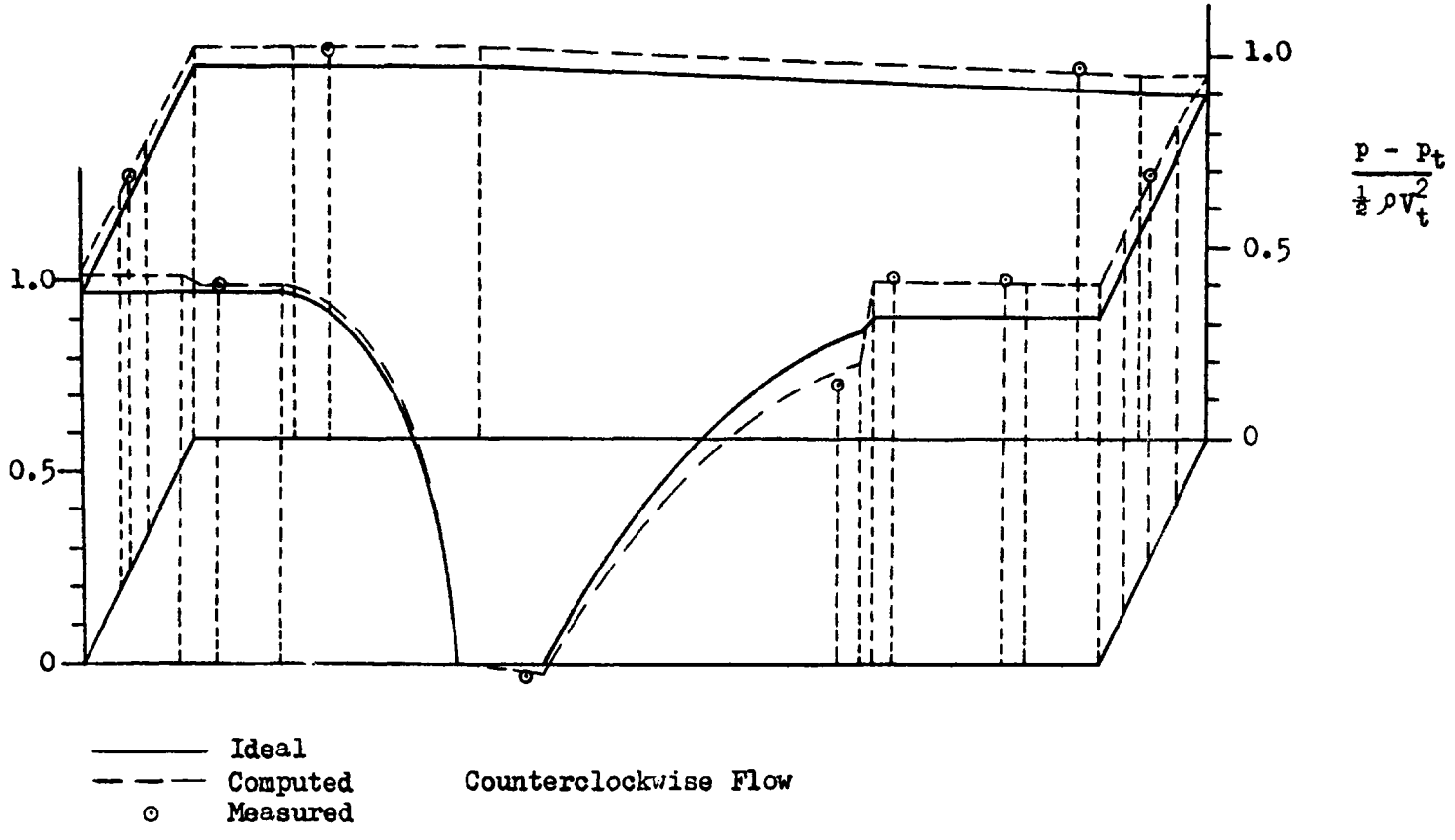

Figure 5.4 Pressure Distribution for Test Section Velocity of 100 fps

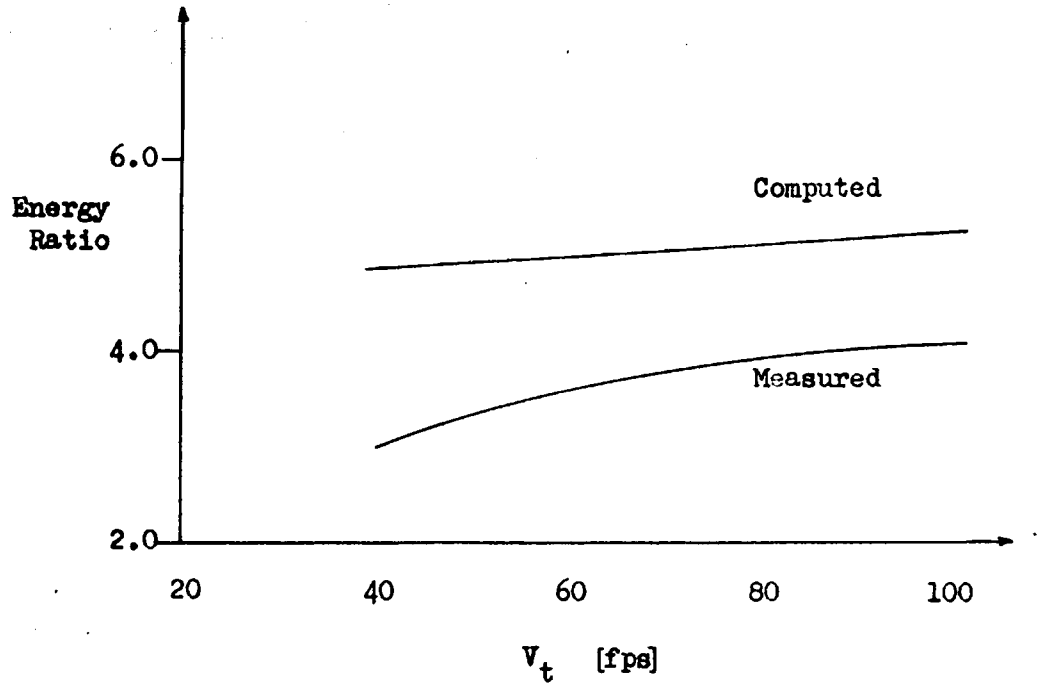

Figure 5.5 Initial Comparison of Computed and Measured Energy Ratio

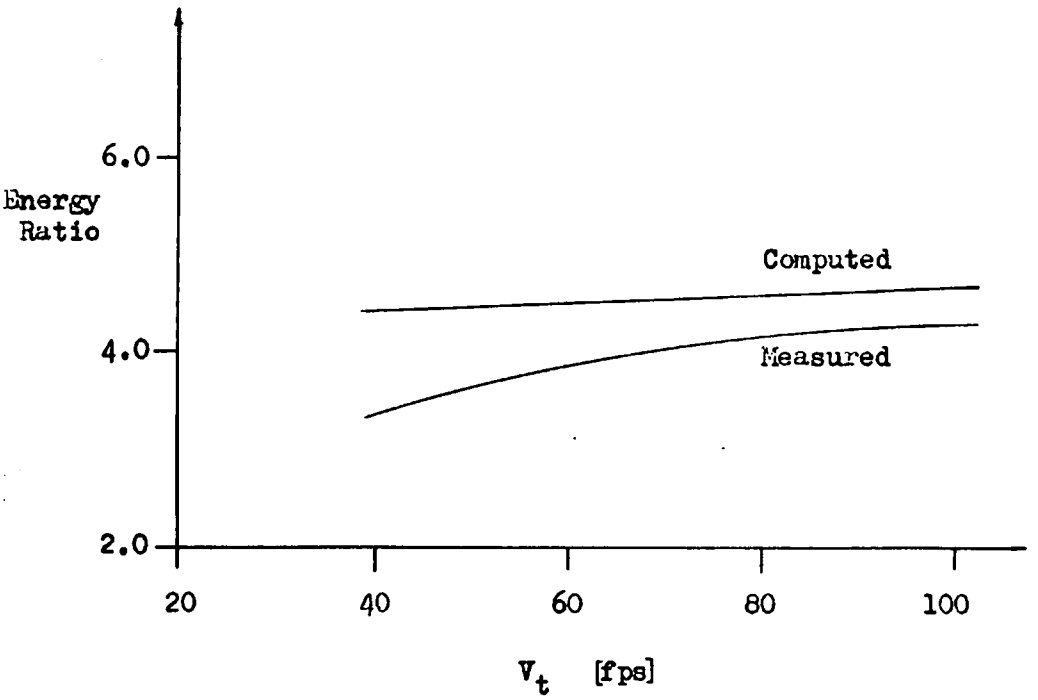

Figure 5.6 Comparison of corrected Energy Ratios

through the section. The bottom of the test section had a 13-inch by 1-1/2 inch slot and eight 3/8-inch diameter holes that were sealed with tape and the junction of the test section to both the nozzle and diffuser were faired with tape. There were seven piezo-taps on each side of the test section and the corners of the test section were mitered with wood. All these surface irregularities tend to invalidate the smooth flow assumption. Since the test section has the highest flow velocity, small errors here greatly affect the energy ratio. To estimate a correction for these two points data taken at 40 fps was used to compute the actual e/De for the test section and the effective area of flow at the end of the diffuser was estimated by subtracting the area of an eight-inch circle from the unobstructed cross-section area. Results of these calculations are shown in Figure 5.6. The corrected values show agreement within 15 per cent of the measured values. Considering the accuracy of the individual measurements, this is satisfactory.

5.6 Conclusions

The nature of surface roughness has a definite effect on energy losses in smaller wind tunnels, so much so that the use of smooth pipe theory can be eliminated from consideration. The key to successful loss estimation

lies in careful evaluation of the nature of the surface roughness. Particularly in the smaller, higher velocity sections the highest value of e, as recorded by Moody, should be used to insure that the losses are not underestimated. Also, it would be reasonable to reduce the estimated energy ratio by 10 to 15 per cent to allow for leaks and joints.

Although the assumption that expansion losses at a divergence and secondary losses at corners are independent of Reynolds number were valid for the range of experiments of this study, the effect of higher velocities on these losses should be investigated before the validity of this method is extended much beyond the range of experiment.

APPENDIX I

SYMBOLS

Letter Symbols

A	Area
D	Diameter
D_e	Equivalent Diameter
e	Absolute Roughness
f	Moody Friction Factor
k	Section Loss Coefficient
K_t	Coefficient of Loss Referred to Jet Energy
L	Length
m	Hydraulic Radius
N_{Re}	Reynolds Number
p	Pressure
P	Perimeter
q	Dynamic Pressure
r	Radius
u	Instantaneous Velocity
V	Average Velocity

Greek Letters

α	Angle of Expansion
β	Equivalent Angle of Expansion
θ	Equivalent Angle of Contraction
κ	Vortex Strength
λ	Flat Plate Friction Coefficient
μ	Dynamic Viscosity
ν	Kinematic Viscosity
ρ	Density
τ	Shear Stress
ϕ	Potential Function
ψ	Stream Function

APPENDIX II

TUNNEL GEOMETRY

This Appendix contains a brief description of the geometry of the one-foot wind tunnel of the Department of Mechanical Engineering, University of Arizona. Sufficient data is included to estimate the performance of the wind tunnel by use of the proposed method.

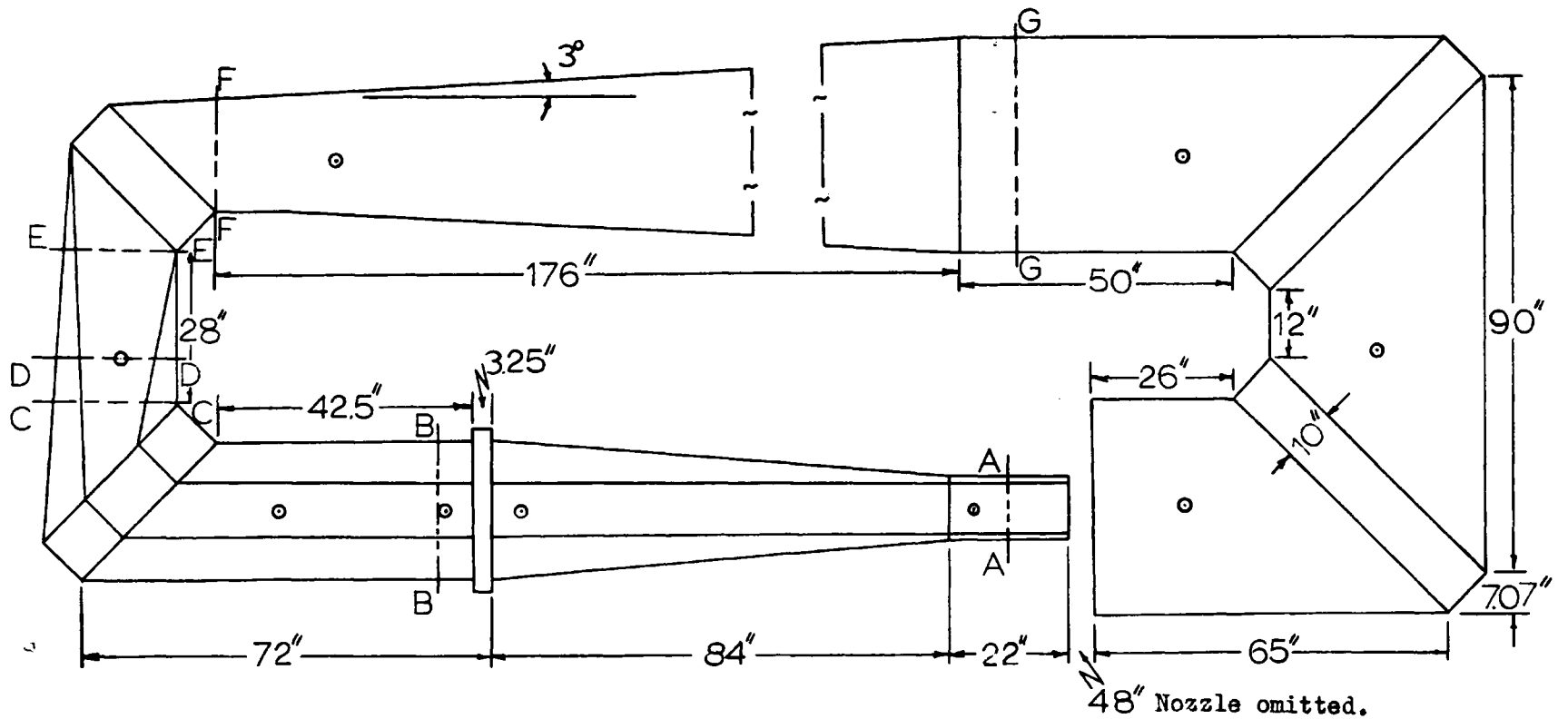

⊙ Indicates location of Piezometric Pressure Taps

Figure II - 1 Side View

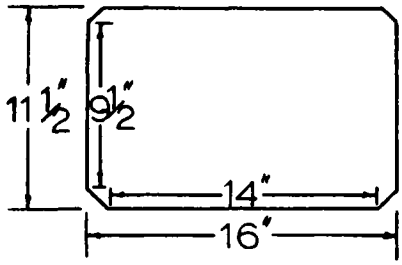

Area 182 sq in

Perimeter 52.6 in

D_e 1.152 ft

Figure II - 2 Section A A

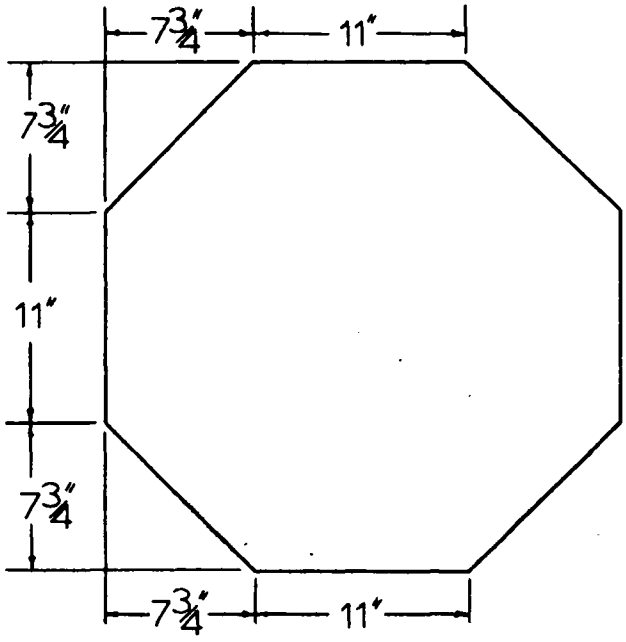

Area 581 sq in

Perimeter 88 in

D_e 2.2 ft

Figure II - 3 Section B B

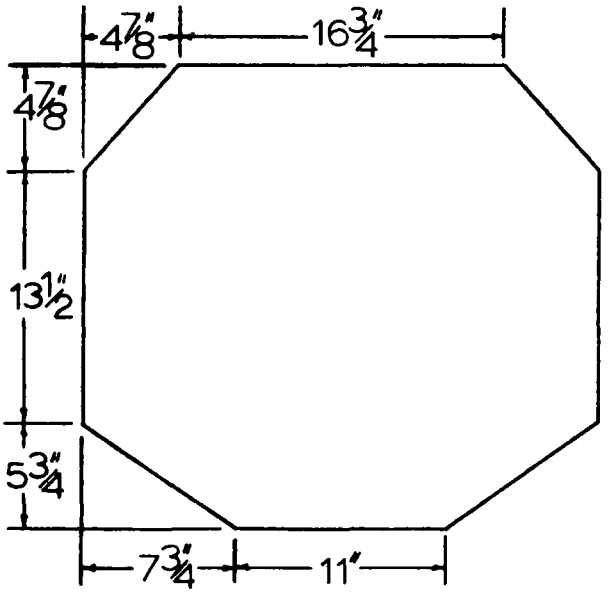

Area 563.6 sq in

Perimeter 87.75 in

D_e 2.14 ft

Figure II - 4 Section C C

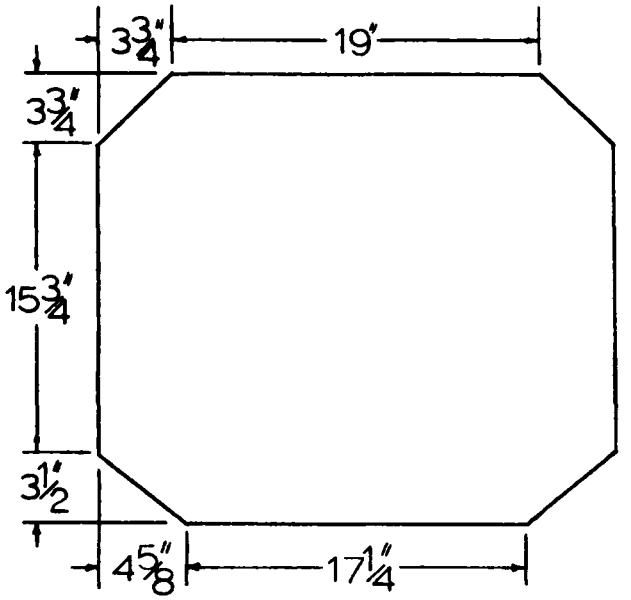

Area 578.8 sq ft

Perimeter 89.75 in

D_e 2.155 ft

Figure II - 5 Section D D

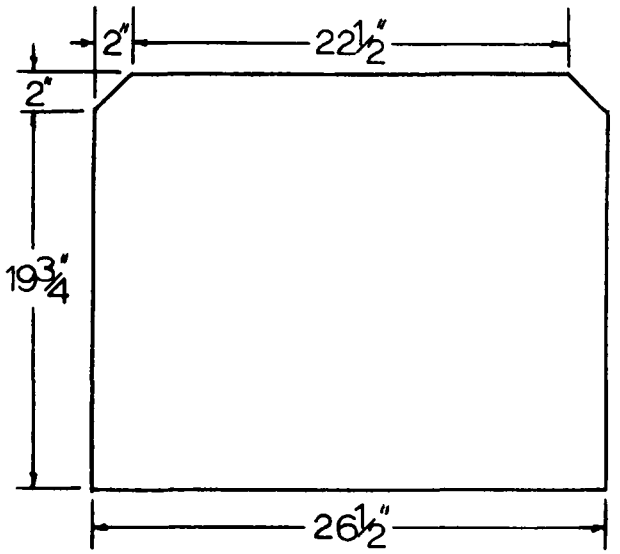

Area 572 sq in

Perimeter 94.5 in

D_e 2.02 ft

Figure II - 6 Section E E

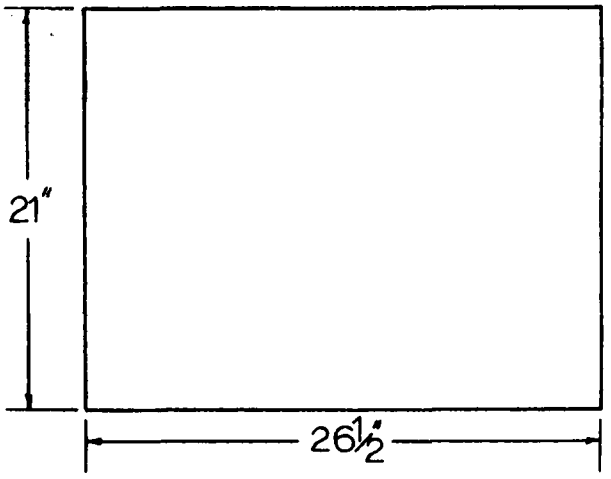

Area 556 sq in

Perimeter 95 in

D_e 1.95 ft

Figure II - 7 Section F F

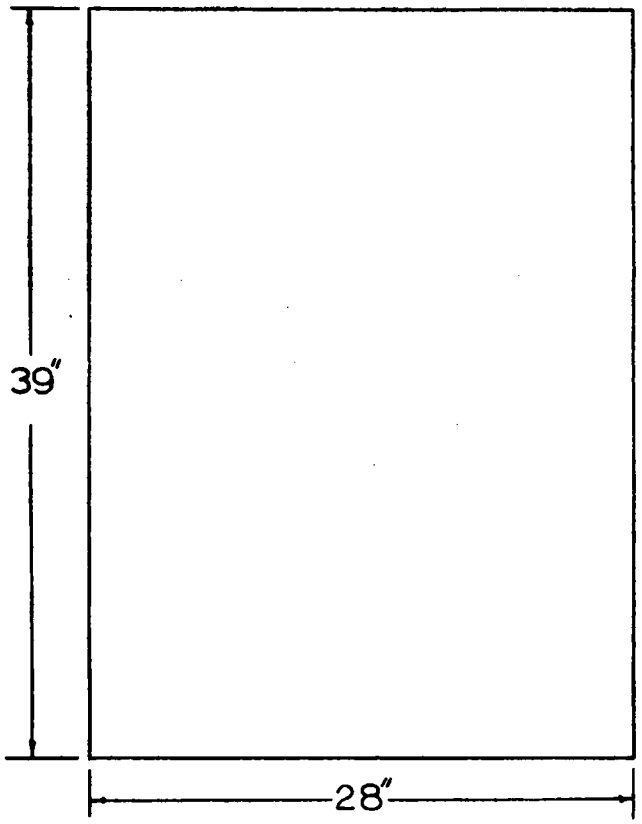

Area 1092 sq in

Perimeter 134 in

D_e 2.72 ft

Figure II - 8 Section G G

APPENDIX III

TABULATION OF CALCULATIONS

Table III-1 Calculations for V_t = 40fps

Section	N_{Re}	f	f_{avg}	K_t	ΣK_t	$1 - \frac{A_t^2}{A^2}$	$\frac{p - p_t}{1/2\ \rho V_t^2}$
Test Section	2.49×10^5	0.0155		0.0247		0.0	-0.0247
Diffuser	(1) 2.49×10^5	0.0224					
	(2) 1.49×10^5	0.0209	0.0217	0.0732	0.0979	0.8828	0.7849
Fan					0.0979	0.9018	1.00929
Cylinder	1.49×10^4	0.0209		0.00353	0.10143	0.9018	1.00576
1st Corner	5.18×10^4			0.01754	0.11897	0.8955	0.98192
Expansion	(1) 1.49×10^5	0.0210					
	(2) 1.46×10^5	0.0210	0.0210	0.00195	0.12092	0.901	0.98547
Contraction	(1) 1.46×10^5	0.0210					
	(2) 1.39×10^5	0.0214	0.0212	0.00013	0.12105	0.8988	0.98314
2d Corner	5.84×10^4			0.01783	0.13898	0.8934	0.95991
Divergence	(1) 1.37×10^5	0.0214					
	(2) 9.76×10^4	0.0210	0.0212	0.00803	0.14691	0.9722	1.03068
Cylinder	9.76×10^4	0.0210		0.00089	0.14780	0.9722	1.02979

Table III-1 (Continued)

Section	N_{Re}	f	f_{avg}	K_t	ΣK_t	$1 - \frac{A_t^2}{A^2}$	$\frac{p - p_t}{1/2\ \rho V_t^2}$
3d Corner	2.99×10^4			0.00501	0.15281	0.9722	1.02478
Cylinder	9.76×10^4	0.0210		0.00022	0.15303	0.9722	1.02456
4th Corner	2.99×10^4			0.00501	0.15804	0.9722	1.01955
Screen				0.0278	0.18584	0.9722	0.99175
Cylinder	9.76×10^4	0.0210		0.00047	0.18631	0.9722	0.99128
Nozzle	(1) 9.76×10^4 (2) 2.49×10^5	0.0183	0.0172	0.01908	0.20539	0	0

Table III-2 Calculations for V_t = 60 fps

Section	N_{Re}	f	f_{avg}	K_t	ΣK_t	$1 - \frac{A_t^2}{A^2}$	$\frac{p - p_t}{1/2\ \rho V_t^2}$
Test Section	3.74×10^5	0.0138		0.0219		0	-0.0219
Diffuser	(1) 3.74×10^5	0.0220					
	(2) 2.24×10^5	0.0202	0.0211	0.0723	0.0942	0.8828	0.7886
Fan					0.0942	0.9018	1.00694
Cylinder	2.24×10^5	0.0202		0.00343	0.09763	0.9018	1.00351
1st Corner	7.77×10^4			0.01707	0.11470	0.8955	0.98014
Expansion	(1) 2.24×10^5	0.0202					
	(2) 2.19×10^5	0.0204	0.0203	0.00190	0.11660	0.901	0.98374
Contraction	(1) 2.19×10^5	0.0204					
	(2) 2.09×10^5	0.0204	0.0204	0.00012	0.11672	0.8988	0.98142
2d Corner	8.76×10^5			0.01719	0.13391	0.8934	0.95883
Divergence	(1) 2.05×10^5	0.0206					
	(2) 1.47×10^5	0.0200	0.0203	0.00893	0.14284	0.9722	1.02870
Cylinder	1.47×10^5	0.0200		0.00085	0.14369	0.9722	1.02785

Table III-2 (Continued)

Section	N_{Re}	f	f_{avg}	K_t	ΣK_t	$1 - \frac{A_t^2}{A^2}$	$\frac{p - p_t}{1/2\ \rho V_t^2}$
3rd Corner	4.48×10^4			0.00479	0.14848	0.9722	1.02306
Cylinder	1.47×10^5	0.0200		0.00020	0.14868	0.9722	1.02286
4th Corner	4.48×10^4			0.00480	0.15348	0.9722	1.01806
Screen				0.02780	0.18128	0.9722	0.99026
Cylinder	1.47×10^5	0.0299		0.00044	0.18172	0.9722	0.98982
Nozzle	(1) 1.47×10^5 (2) 3.74×10^5	0.0170 0.0148	0.0159	0.01762	0.19934	0	0

Table III-3 Calculations for V_t = 80 fps

Section	N_{Re}	f	f_{avg}	K_t	ΣK_t	$1 - \frac{A_t^2}{A^2}$	$\frac{p - p_t}{1/2\ \rho V_t^2}$
Test Section	4.89×10^5	0.0130		0.0207		0	-0.0207
Diffuser	(1) 4.89×10^5	0.0220					
	(2) 2.89×10^5	0.0200	0.0210	0.0721	0.0928	0.8828	0.7900
Fan					0.0928	0.9018	1.00470
Cylinder	2.89×10^5	0.0200		0.0034	0.0962	0.9018	1.00130
1st Corner	1.04×10^5			0.01665	0.11285	0.8955	0.97845
Expansion	(1) 2.98×10^5	0.0200					
	(2) 2.92×10^5	0.0200	0.0200	0.00187	0.11472	0.901	0.98198
Contraction	(1) 2.92×10^5	0.0200					
	(2) 2.78×10^5	0.0202	0.0201	0.00012	0.11484	0.8988	0.97966
2nd Corner	1.17×10^5			0.01680	0.13164	0.8934	0.95746
Divergence	(1) 2.74×10^5	0.0204					
	(2) 1.95×10^5	0.0197	0.0201	0.00891	0.14055	0.9722	1.02735
Cylinder	1.95×10^5	0.0197		0.00084	0.14139	0.9722	1.02651

TABLE III-3 (Continued)

Section	N_{Re}	f	f_{avg}	K_t	ΣK_t	$1 - \frac{A_t^2}{A^2}$	$\frac{p - p_t}{1/2\ \rho V_t^2}$
3d Corner	5.98×10^4			0.00467	0.14606	0.9722	1.02184
Cylinder	1.95×10^5	0.0197		0.00021	0.14627	0.9722	1.02163
4th Corner	5.98×10^4			0.00467	0.15094	0.9722	1.01696
Screen				0.02780	0.17874	0.9722	0.98916
Cylinder	1.95×10^5	0.0197		0.00044	0.17918	0.9722	0.98872
Nozzle	(1) 1.95×10^5 (2) 4.98×10^5	0.0156 0.0141	0.0149	0.01652	0.19570	0	0

Table III-4 Calculations for V_t = 100 fps

Section	N_{Re}	f	f_{avg}	K_t	ΣK_t	$1 - \frac{A_t^2}{A^2}$	$\frac{P - P_t}{1/2\ \rho V_t^2}$
Test Section	6.23×10^5	0.0125		0.0199		0	-0.0199
Diffuser	(1) 6.23×10^5	0.0215					
	(2) 3.72×10^5	0.0198	0.0207	0.0717	0.0916	0.8828	0.7912
Fan					0.0916	0.9018	1.00106
Cylinder	3.72×10^5	0.0198		0.00336	0.09496	0.9018	0.99770
1st Corner	1.3×10^5			0.01633	0.11129	0.8955	0.97507
Expansion	(1) 3.72×10^5	0.0198					
	(2) 3.65×10^5	0.0198	0.0198	0.00176	0.11305	0.901	0.97881
Contraction	(1) 3.65×10^5	0.0198					
	(2) 3.48×10^5	0.0200	0.0199	0.00012	0.11317	0.8988	0.97649
2d Corner	1.46×10^5			0.01653	0.12970	0.8934	0.95456
Divergence	(1) 3.42×10^5	0.0200					
	(2) 2.44×10^5	0.0194	0.0205	0.00900	0.13870	0.9722	1.02436
Cylinder	2.44×10^5	0.0194		0.00083	0.13953	0.9722	1.02353

Table III-4 (Continued)

Section	N_{Re}	f	f_{avg}	K_t	ΣK_t	$1 - \frac{A_t^2}{A^2}$	$\frac{p - p_t}{1/2\ \rho V_t^2}$
3d Corner	7.47×10^4			0.00458	0.14411	0.9722	1.01895
Cylinder	2.44×10^5	0.0194		0.00020	0.14431	0.9722	1.01875
4th Corner	7.47×10^4			0.00458	0.14431	0.9722	1.01317
Screen				0.02502	0.14889	0.9722	0.98915
Cylinder	2.44×10^5	0.0194		0.00043	0.17391	0.9722	0.98782
Nozzle	(1) 2.44×10^5 (2) 6.23×10^5	0.0155 0.0142	0.0149	0.01652	0.19086	0	0

APPENDIX IV

EXPERIMENTAL DATA

In the following tables the pressure taps are located as indicated below:

Pressure Tap 1 - Pitot tube in test section (static tap)

2 - End of test section

3 - End of diffuser

4 - After fan

5 - Before 1st corner

6 - Between 1st and 2d corner

7 - After 2d corner

8 - Before 3d corner

9 - Between 3d and 4th corner

10 - After 4th corner

Table IV-1 Data for V_t = 40 fps

Pressure Tap	h [in]	$h - h_1$ [in]	$\frac{p - p_t}{1/2\ \rho V_t^2}$
1	6.22	0	0
2	6.25	-0.03	-0.04
3	5.69	0.53	0.707
4	5.43	0.79	1.053
5	5.46	0.76	1.014
6	5.48	0.74	0.988
7	5.48	0.74	0.988
8	5.41	0.81	1.080
9	5.42	0.80	1.068
10	5.48	0.74	0.988

T_a = 81 F, p_a = 27.5 in Hg, q_t = 0.32 in H_2O

Table IV-2 Data for V_t = 60 fps

Pressure Tap	h [in]	$h - h_1$ [in]	$\frac{p - p_t}{1/2\ \rho V_t^2}$
1	6.04	0	0
2	6.09	-0.04	-0.024
3	4.82	1.22	0.706
4	4.32	1.69	0.994
5	4.37	1.67	0.982
6	4.39	1.65	0.970
7	4.42	1.62	0.953
8	4.32	1.72	1.012
9	4.33	1.71	1.006
10	4.39	1.65	0.970

T_a = 81 F, p_a = 27.55 in Hg, q_t = 0.73 in H_2O

Table IV-3 Data for V_t = 80 fps

Pressure Tap	h [in]	$h - h_1$ [in]	$\frac{p - p_t}{1/2\ \rho V_t^2}$
1	7.19	0	0
2	7.29	-0.10	-0.033
3	5.00	2.19	0.723
4	4.14	3.05	1.007
5	4.16	3.03	1.000
6	4.22	2.97	0.980
7	4.29	2.90	0.956
8	4.11	3.08	1.018
9	4.12	3.07	1.012
10	4.20	2.99	0.986

T_a = 81 F, p_a = 27.55 in Hg, q_t = 1.30 in H_2O

Table IV-4 Data for V_t = 100 fps

Pressure Tap	h [in]	$h - h_1$ [in]	$\frac{p - p_t}{1/2\ \rho V_t^2}$
1	8.65	0	0
2	8.76	-0.11	-0.0234
3	5.20	3.45	0.734
4	3.91	4.74	1.008
5	3.92	4.73	1.006
6	4.03	4.61	0.980
7	4.10	4.54	0.975
8	3.87	4.78	1.018
9	3.88	4.77	1.014
10	4.00	4.65	0.989

T_a = 81 F, p_a = 27.55 in Hg, q_t = 2.02 in H_2O

REFERENCES

1. Wattendorf, Frank L., "Factors Influencing the Energy Ratio of Return Flow Tunnels," Proceedings of the Fifth International Congress for Applied Mechanics, Cambridge, 1938.

2. Streeter, Victor L., Fluid Mechanics, Second Edition, McGraw-Hill Book Company, Inc., 1958.

3. Moody, L. F., "Friction Factors for Pipe Flow," Transactions of the American Society of Mechanical Engineers, Vol. 66, 1944.

4. Skoglund, V. J., "Effect of Roughness of the Coefficient of a Closed Channel," Journal of the Aeronautical Sciences, Vol. 4, October 1936.

5. Pipe, Alan, Wind Tunnel Testing, Second Edition, John Wiley and Sons., Inc., New York, 1958.

6. Tsein, Hsue-Shen, "On the Design of a Contraction Cone for a Wind Tunnel," Journal of the Aeronautical Sciences, Vol. 10. 21 September 1942.

7. Szczeniowski, Boleslaw, "Contraction Cone for a Wind Tunnel," Journal of the Aeronautical Sciences, Vol. 10, October 1943.

8. Krober, G., "Guide Vanes for Deflecting Fluid Currents with Small Loss of Energy," Technical Memoranda of the National Advisory Committee for Aeronautics, No. 722, September 1933.

9. Winters, K. G., "Comparative Tests of Thick and Thin Turning Vanes in the RAE 4x3 Foot Wind Tunnel," Reports and Memoranda of the British Air Research Committee, No. 2589, 1947.

10. Schlichting, Herman, Boundary Layer Theory, Fourth Edition, McGraw-Hill Book Company, Inc., 1960.

11. Tripp, Wilson, "Friction Losses in an Artifically Roughened Rectangular Channel," Journal of the Aeronautical Sciences, Vol. 4, November 1936.

12. Darrius, G., "Some Factors Influencing the Design of the Wind Tunnels," Brown-Boveri Review, Vol. 30, No. 7/8, July-August 1943, pp. 168-176.

13. Olson, R. M., Essentials of Engineering Fluid Mechanics, International Textbook Company, 1962.

14. Streeter, Victor L., Fluid Dynamics, McGraw-Hill Book Company, Inc., 1948.

15. Milne-Thompson, L. M., Theoretical Hydrodynamics, Fourth Edition, The Macmillan Company, New York, 1960.